J Ind Microbiol Biotechnol (2009) 36:787–800
DOI 10.1007/s10295-009-0552-9

ORIGINAL PAPER

Morphological quantification of filamentous fungal development using membrane immobilization and automatic image analysis

David J. Barry · Cecilia Chan · Gwilym A. Williams

Received: 25 November 2008 / Accepted: 17 February 2009 / Published online: 7 March 2009

Abstract Mycelial morphology is a critically important process property in industrial fermentations of filamentous micro-organisms, as particular phenotypes are associated with maximum productivity. However, the accurate quantification of complex morphologies still represents a significant challenge in elucidating this relationship. A system has been developed for high-resolution characterisation of filamentous fungal growth on a solid substrate, using membrane immobilization and fully-automatic plug-ins developed for the public domain, Java-based, image-processing software, ImageJ. The system has been used to quantify the microscopic development of *Aspergillus oryzae* on malt agar, by measuring spore projected area and circularity, the total length of a hyphal element, the number of tips per element, and the hyphal growth unit. Two different stages of growth are described, from the swelling of a population of conidiospores up to fully developed, branched hyphae 24 h after inoculation. Spore swelling expressed as an increase in mean equivalent spore diameter was found to be approximately linear with time. Widespread germination of spores was observed by 8 h after inoculation. From approximately 12 h, the number of tips was found to increase exponentially. The specific growth rate of a population of hyphae was calculated as approximately 0.24–0.27 h^{-1}. A wide variation in growth kinetics was found within the population. The robustness of the image-analysis system was verified by testing the effect of small variations in the input data.

Keywords Fungal morphology · Membrane immobilization · Automatic image analysis · Growth kinetics · Solid-state fermentation

D. J. Barry · G. A. Williams (✉)
School of Biological Sciences, Dublin Institute of Technology, Kevin Street, Dublin 8, Ireland
e-mail: gwilym.williams@dit.ie

D. J. Barry
e-mail: david.barry@dit.ie

C. Chan
Centre for the Advancement of University Teaching, University of Hong Kong, Pokfulam, Hong Kong

Introduction

Microscopic examination of filamentous fungi using a stain and wet-mount procedure is a cornerstone of medical mycology and has centred on the diagnostic value of characteristic reproductive structures as an aid to identification of specific genera. Integral to the performance of such tests has been the evolution of improved sampling methods that preserve the natural architecture of the fungus [1, 2] and allow microscopic examination and interpretation by use of the unaided human eye. Such simple methods are of equal value in biotechnology during new strain isolation and identification and routine monitoring of morphology as a component of cell banking. However, the needs of the microbial physiologist during the design of industrial biomanufacturing processes are focussed on optimizing a reproducible relationship between biomass and metabolite production in axenic culture, and often in submerged systems in which a vegetative mycelium predominates. The specific form adopted by the fungus may be because of a combination of the type of bioreactor used (submerged, solid state, or mixed phase), the culture mode (batch, fed-batch, or continuous), and the physicochemical conditions employed during the fermentation, and often requires a consideration of micro and macro-morphological phenotypes.

The critical importance of filamentous fungi in the industrial production of antibiotics and enzymes is now being consolidated by their exploitation in additional food and pharmaceutical biotechnology uses. Reflecting a saprophytic mode of nutrition, filamentous fungi demonstrate naturally high levels of extracellular hydrolase secretion, and efforts are ongoing to exploit this capability for efficient heterologous protein expression [3]. Similarly, genome-sequencing projects for a variety of industrial fungi are either complete or well underway [4], and taken together with greatly improved methods for genetic transformation, hold substantial promise for new product development based on recombinant DNA approaches. Many fungi have GRAS ("generally regarded as safe") status (US Food and Drug Administration), and are able to grow well on inexpensive agricultural waste products. Efforts to metabolically engineer biochemical pathways for protein glycosylation into fungi are also showing promise [5], an essential step enabling their more widespread use as recombinant hosts for the expression of human pharmaceutical proteins. It has long been recognised that solid-state culture has inherently higher productivity potential compared with submerged culture systems [6]. However, reports of differential gene expression in fungi growing in liquid and solid-phase culture formats [7–11] now open up the possibility for industry to build on established bioprocess technology know-how, permitting a revisionist approach to the screening of existing fungal cell banks for new metabolites.

Despite such progress, a significant hurdle remains in elucidating the precise relationship between fungal morphology and productivity in industrial fermentation processes, a complex interplay of the variety of cohesive and disintegrative forces operating in any specific fermentation process [12]. At the microscopic level, there is evidence to suggest that extracellular protein yield is positively correlated with increased numbers of actively growing hyphal tips [13–15], and this points to the selection of bioprocess conditions that favour increased branching. At the sub-cellular level, vacuolation has been related to citric acid production in *Aspergillus niger* [16], and it has also been shown that apical length, hyphal diameter, and concentration of cell nuclei in *A. oryzae* and *A. niger* change in response to variations in substrate concentration [17].

At the macroscopic level, a variety of phenotypes may be manifested, spanning dispersed mycelia to mycelial aggregates in the form of irregular clumps or more organized pellets that may vary in diameter, core density, and perimeter circularity [18]. Although some studies have failed to demonstrate a direct correlation between morphology and metabolite yield [15, 19], many reports indicate a reproducible relationship at the macro-morphological level. Accordingly, the mycelial form has been found to be optimum for production of such diverse metabolites as fumaric acid by *Rhizopus arrhizus* [20] and penicillin by *Penicillum chrysogenum* [3]. Conversely, pellets were found to be the preferred morphology for production of glucose oxidase [21], polygalactonuronidase [22], and glucoamylase [23] in *A. niger* fermentations. Indeed, contradictory reports exist in the case of the production of citric acid from *A. niger* [24, 25], but this disagreement may result from ambiguous classification of fungal conformations in earlier studies, because of a lack of image-analysis methods to quantify morphology. The picture is further complicated by the fact that fungal morphology also influences the rheological properties of a fermentation broth, which in turn influences the transport of nutrients within the bioreactor [26]. In contrast to pellets, the filamentous form causes the broth to exhibit non-Newtonian, pseudo-plastic behaviour, which leads to mixing problems and limitations in oxygen and heat transfer; higher power inputs are therefore required for this growth form, to facilitate adequate mixing of the broth. Conversely, there is an optimum maximum pellet size, beyond which oxygen transfer to the interior becomes a limiting factor and autolysis begins [27, 28].

The need to precisely quantify morphological variation in vegetative mycelium as a control component of bioprocess performance has led to the deployment of computer-aided image analysis as a tool for the study of submerged [18] and solid state [29] culture systems. Measurements which offer comparative value at the microscopic level include total hyphal length, hyphal growth unit (ratio of total hyphal length to the total branch number [30]) and the number of tips [31–34]. Macroscopic factors have included discriminators such as projected area, circularity, eccentricity, and fractal dimension [32, 35–38].

We recently reported proof-of-principle of a new method that enables high magnification, microscopic examination of hyphal conformations in their natural state [39]. The fungus is grown on a cellulose-derivative membrane placed on top of a solid nutrient substrate, and is then processed for microscopy by staining, drying, and rendering the membrane transparent by treatment with mineral oil. The objective of this study was to further define the optimum operational conditions for this assay, in conjunction with the development of a new automatic image-analysis suite using the publicly available ImageJ software. Using the industrially important filamentous fungus *A. oryzae* as a model organism, we report the utility of the system for quantitative characterization of spore germination and early stage hyphal development in solid state culture.

Materials and methods

Microorganism maintenance and preservation

Conidiospores of *A. oryzae* (ATTC 12891) were harvested from malt agar (Lab M) slant cultures (incubated for seven days at 25°C) by addition of 5 ml phosphate-buffered saline (PBS; pH 7.2, Oxoid Dulbecco "A"; 0.85% w/v) containing Tween 80 (0.1% v/v). Conidiospores were dislodged using a sterile swab, briefly mixed, and the suspension was filtered through a sterile Nylon net filter (Millipore NY1104700; 11 μm pore size) to remove hyphae. Conidium concentration was standardized using a Neubauer chamber to yield a stock concentration of 1×10^6 conidia ml^{-1} and aliquots were stored in glycerol (20% v/v) at −20°C. The viability of spores after freezing was found to be 36 ± 2% of stock concentration (pour plate method, malt agar, 24–48 h incubation, average of three separate determinations).

Cell immobilization and microorganism cultivation

The basic conidiospore immobilization procedure used for standardization experiments consisted of filtering a suspension (25 ml of approximately 400 spores ml^{-1}) through a cellulose nitrate membrane (Sartorius Stedim 11306-47-ACN) using a membrane filtration device (Millipore) connected to a vacuum pump. A spore concentration of this magnitude was found by trial-and-error to be optimum in preventing over-crowding of mycelium on the membrane upon germination, while suspension volumes in excess of 20 ml were adequate to ensure a uniform spore coverage of the membrane. After washing with PBS–Tween 80 (for removal of any wall-adherent cells) and sterile water (removal of excess PBS–Tween 80), the membrane was overlaid evenly on to the surface of malt agar and incubated at 25°C.

Processing of culture for image analysis

In the optimized procedure derived from the experiments described below, the membrane was removed from the agar after a suitable period of time and replaced in a filtration device where it was exposed to fixative solution (phenol 20% w/v, glycerol 40% v/v, lactic acid 20% v/v in distilled water) for 5 min. Following washing with PBS–Tween 80 and then water, the membrane was placed in a Petri dish and dried at 65°C (75 min). After staining with lacto-phenol cotton blue (Pro-Lab Diagnostics), the membrane was rinsed with PBS–Tween 80 (5 min) and distilled water, followed by cutting and mounting on a microscope slide and drying at 65°C (75 min). The membrane was rendered transparent and suitable for imaging by treatment with microscopy immersion oil (Olympus AX 9602).

Microscopy and image capture

A PowerShot S50 digital camera (Canon) fitted to a DM LS2 light microscope (Leica) was controlled remotely from a desktop PC using the RemoteCapture utility (Canon). Colour images (640 × 480 or 1600 × 1200 pixels) were captured at magnifications of ×1,000 (for qualitative analysis), ×200 or ×100, yielding a resolution of approximately 1 μm per pixel for images of hyphae and 0.2 μm for spores. Inter-pixel distances were determined by imaging a stage graticule. Images were stored in JPEG format with minimum image compression.

Image analysis

Image analysis plug-ins were developed for the public domain, Java-based image processing program, ImageJ v1.39d (US National Institutes of Health), to enable the quantitative analysis of the fungus. The software begins by requesting a set of data for the analysis from the user, together with the directory in which the bank of images to be analysed is contained. The analysis then proceeds automatically until all the images in the specified directory have been analysed. The process for each individual image is outlined as follows (Fig. 1).

Image pre-processing begins with filtering of the image to compensate for low-frequency, uneven illumination, which can result in shading and a non-uniform background. This complicates the segmentation process as grey levels may exist within the image that are common to both object and background and selecting a single threshold level at which to separate the two may therefore not be possible. Applying a grey-level threshold to such an image will result in a high level of artefact.

Variations in the background grey level can be corrected by treating the image as a 2D signal and subjecting it to high-pass filtering, which is implemented using ImageJ's in-built "Bandpass Filter" function. This removes image noise by Gaussian filtering in Fourier space, the radius of the filter being set to the pixel equivalent of 40 μm (40 pixels for images of hyphae, 200 pixels for spores), which is large relative to the width of a typical hypha (approximately 2–4 μm). Any high-frequency speckle noise is subsequently removed by median filtering.

The image is then divided into three, 8-bit grey-scale images, representing the three primary colour components (red, green, and blue). The red component exhibits the greatest contrast for images of lacto-phenol cotton blue-stained samples and is retained for image processing; the green and blue components are discarded. A grey-level threshold, calculated by ImageJ using the iso-data algorithm, is now applied, resulting in a binary image.

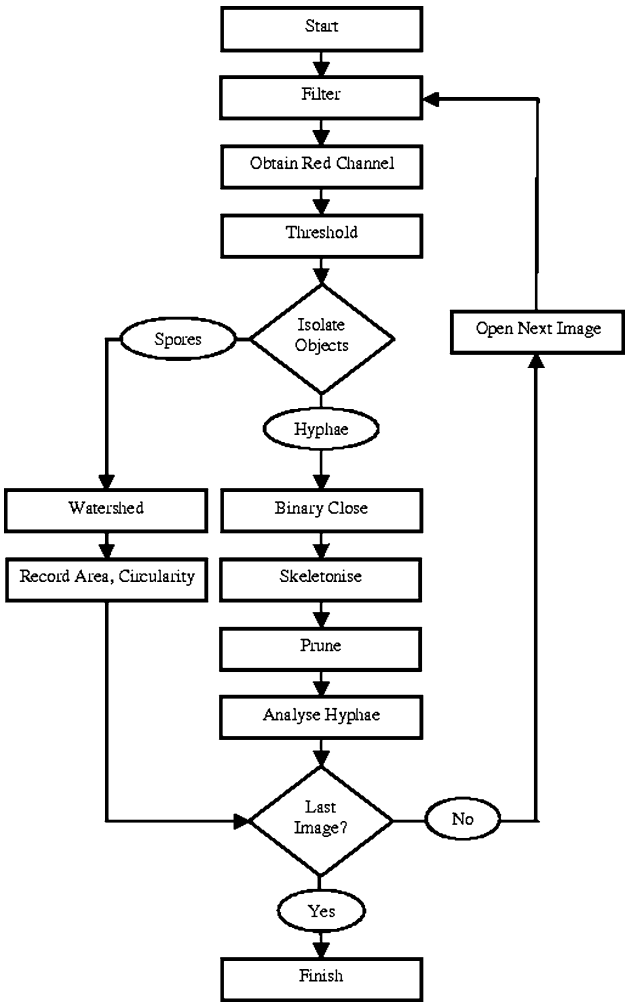

Fig. 1 Algorithm used for characterization of fungal micromorphology

The next stage of the routine depends on whether spores or hyphae are the primary object of study. It is unlikely that viable spores and hyphae will be present in the same image: results from this study indicated that most spores had germinated by approximately 8 h after inoculation (data not shown). Any spores present in a sample taken after this time are considered to be non-viable and are treated by the system as artefacts.

In the case of spores, the "Watershed" function is used to separate any touching objects. ImageJ's "Particle Analyser" is then used to classify objects based on area (A) and circularity (C), with the latter being defined as follows:

$$C = \frac{4.\pi.A_P}{P^2}$$

where A_p is the projected area of the object in question and P is the measured perimeter. In the case of a circle, $A_p = \pi r^2$ and $P = 2\pi r$, and so $C = 1$. The larger P becomes with respect to A_p, the less circular the object becomes and so the value of C decreases. Spores of many industrially relevant fungi, for example *Aspergillus*, are relatively spherical [33]. Objects with a projected area above a specified minimum ($A_{p,min}$) and with a circularity greater than a threshold value ($C_{s,min}$) are considered to be spores; remaining objects are considered to be artefacts and are excluded from the analysis. Once identified, the projected area and circularity of spores are recorded and the algorithm proceeds to the next image in the folder.

When hyphae are the objects of interest, a single binary "close" operation (a single dilation operation followed by a single erosion) is performed to remove any small breaks (or holes) in the objects. The "Particle Analyser" is then used to identify all objects with a projected area above $A_{p,min}$ and with a circularity less than a second threshold value ($C_{h,max}$). Objects that do not meet these criteria are excluded from the analysis. The binary image of the hyphal elements is then skeletonised, which reduces the objects in the image to a series of lines one pixel in width.

The "skeletonisation" of an object during image analysis can occasionally result in artefactual points or branches [35, 40]. Artefactual points (sites where the skeleton is greater than one pixel in width) can lead to the incorrect classification of branch-points, while artefactual branches can lead to an over-estimation of hyphal length and the number of hyphal tips. These may be removed by way of "pruning" (Fig. 2), which also has the effect of removing any remaining small artefacts from the image.

The routine begins by scanning the image in a raster fashion until a black pixel is located. If this pixel is deemed artefactual (by way of a look-up table), it is removed. This process continues until the end of the image has been reached.

The second stage begins by scanning the image in a raster fashion until a hyphal tip is located. A tip is defined as a black pixel with just one other black pixel in the immediate neighbourhood (Fig. 3). The location of the tip is recorded and the skeleton is then traced from this tip along the hyphal length until either another tip or branch-point is reached. A branch-point is defined as a black pixel with three or more black pixels in the immediate neighbourhood, with no two of these neighbours joined. The length of the branch is then calculated on the basis of the number of pixels traversed. If the length of the branch is less than the specified minimum ($L_{b,min}$) it is removed. The scan of the image then proceeds from the point where the initial tip was located and the process continues until the end of the image has been reached.

Once pruned, the skeletonised hyphae are suitable for analysis (Fig. 4). The routine begins by scanning the image in a raster fashion until a hyphal tip is located. The location of the tip is noted and the skeleton is then traced from this tip along the hyphal length until either another tip or

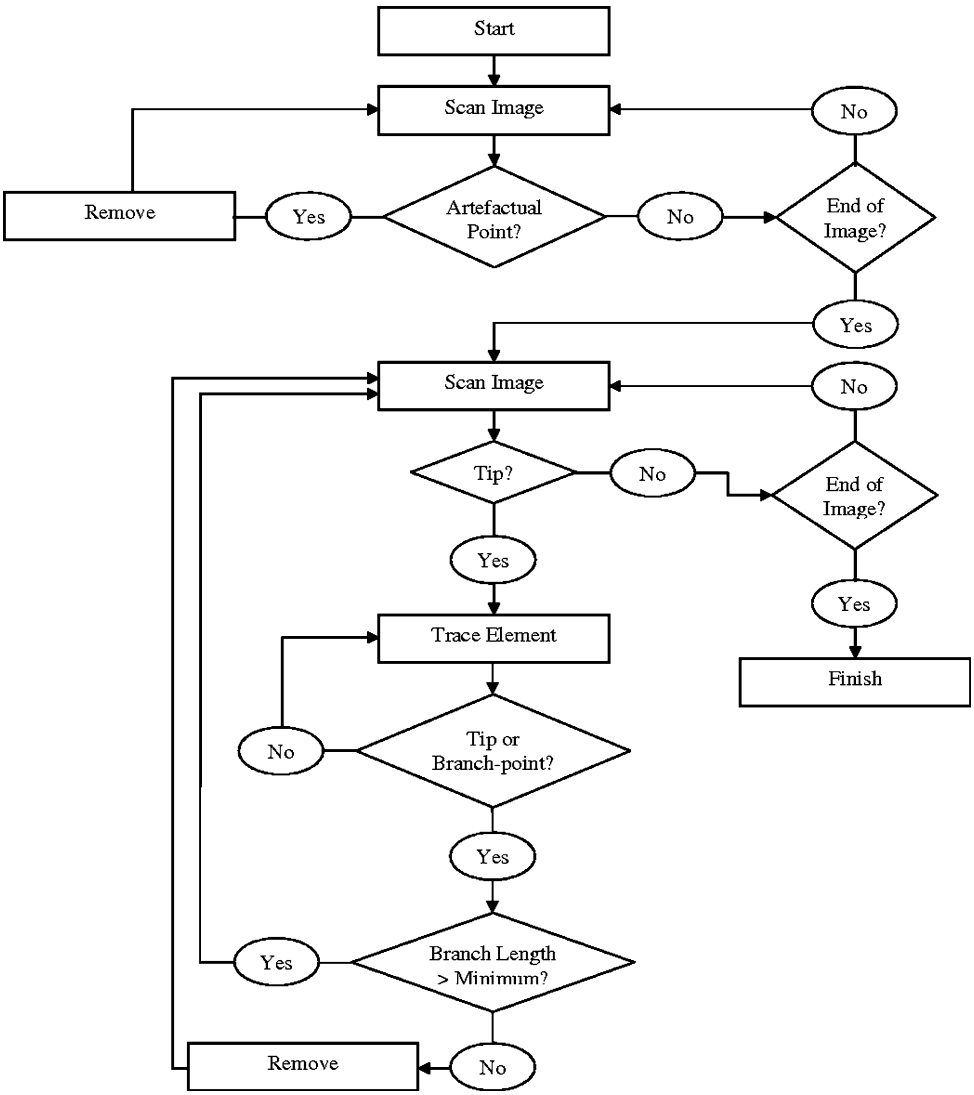

Fig. 2 Algorithm used for the pruning of skeletal hyphal structures prior to measurement

branch-point (collectively termed "end-points") is reached. At this point, the length of the branch is recorded, along with the positions and classification of the end-points. This combined information describes a hyphal "segment". For example, un-branched hyphae will consist of a single segment with two tips as end-points.

If a branch-point is located, tracing continues along the first segment found branching away from this point; any additional segments branching from this point are pushed on to a stack, containing segments yet to be traced. If a hyphal tip is reached, the current segment is recorded and the most recently encountered, non-traced segment is "popped" from the top of the stack, and the routine continues tracing from there.

If a tip is reached and all segments in the current hyphal element have been traced, the measured data (total hyphal length, number of tips, and hyphal growth unit) are output to the results table. The algorithm then returns to the point in the image where the last hyphal element was first located and continues to scan until either another element is detected or the end of the image is reached. When all elements in the image have been analysed, the routine moves on to the next image in the folder.

Validation of image-analysis system

Semi-automatic image analysis was also performed to validate the automatic system. Noise removal was performed according to the automatic method. Grey-level thresholding and selection of hyphal elements from the image were both performed manually, as was artefact removal and the filling of any breaks or holes in the hyphal elements. The elements were then skeletonised and analysed according to the automatic method; the pruning of the skeleton was omitted from the semi-automatic method as artefact removal was performed prior to skeletonisation.

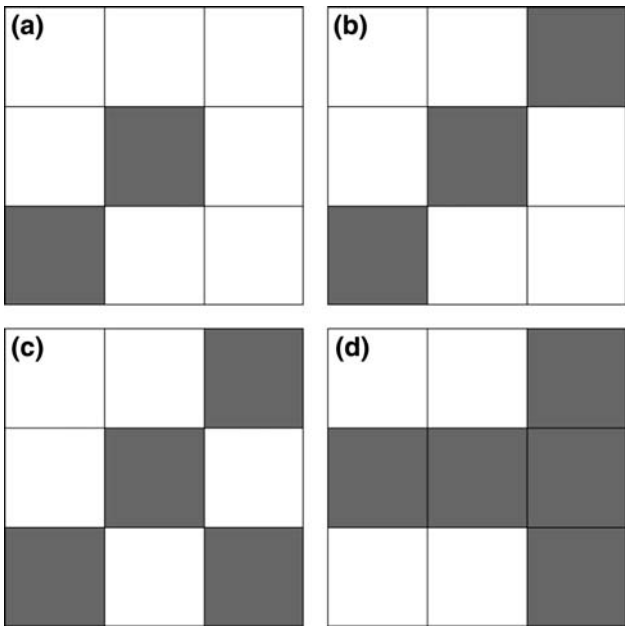

Fig. 3 Classification of points on a skeletal hyphal structure. **a** A pixel is defined as a hyphal tip if all but one of the neighbouring pixels is *white*. **b** If two of the neighbouring pixels are *black*, the current pixel is deemed an internal component of a hyphal segment. **c** A branch-point is defined if at least three neighbouring pixels that do not share a common edge are *black*. **d** Conjoined neighbouring *black* pixels indicate the current pixel is adjacent to a branch-point

Visualisation of fungal morphology

We have recently reported the general utility of cellulose nitrate membranes in the microscopic examination of fungal morphology, enabling high-power magnification of images in a largely two-dimensional format [39]. Further development of the system was undertaken in parallel with the development of the image-analysis software with a view to optimizing overall system resolution, specificity and speed of execution.

Contiguous staining of hyphal elements is essential to avoid misinterpretation of the field of view by the image-analysis system. Staining of membranes while still wet was found to result in non-uniform, patchy staining of hyphae (Fig. 5), which in turn resulted in an over-estimation of the number of discrete hyphal elements within a given sample and underestimation of hyphal length and number of tips. Within a typical experiment, it was found that up to 80% ($n = 50$) of the hyphal elements were misinterpreted as multiple objects by ImageJ within samples that were stained while wet. Drying of membranes before staining reduced the incidence of this artefact to less than 2% of cases.

Within certain limits of time and temperature, the drying of membranes was not found to adversely affect cell morphology. Drying at 25°C for 24 h was without significant effect on spore size, but prolonged exposure (up to 72 h) resulted in a reduction of the mean projected area of the spore population (approximately 8%; Table 1). The drying of samples at temperatures up to 105°C had no significant impact on spore morphology if performed for a short time (10 min) but caused the cellulose nitrate membrane to wilt. No significant change in spore circularity was observed with any treatment. A drying treatment of 65°C for 1.25 h was selected for routine use; this enabled acceptable speed of processing without compromising cell morphology or the integrity of the membrane.

An important caveat to the use of drying procedures is that a fixative be employed to maintain cell structure. Apparent rupturing of hyphal tips was observed in non-fixed samples that were dried prior to staining, with the effect being most pronounced when samples were dried at 65°C (Fig. 6). This rendered hyphal elements unsuitable for analysis, because the affected tips were incorrectly classified by the image-analysis system. Typically it was found that approximately 60% ($n = 70$) of hyphal elements exhibited at least one ruptured tip when dried at 65°C, but when samples were fixed before drying (using phenol–glycerol–lactic acid), this figure was reduced to approximately 5% (data not shown). Exposure to lacto-phenol cotton blue or fixative caused the membrane to wilt slightly on contact, but extended exposure (up to 30 min) was not found to have any additional effect. The optimised method is presented in flowchart form (Fig. 7).

Results

Kinetics of spore swelling

The optimised system was used to study the development of *A. oryzae* spores germinating on malt agar. A time course from 0 to 8 h was performed with $A_{p,min}$ set to 3 μm^2 and $C_{s,min}$ set to 0.8 (Fig. 8). Similar to the value for *A. oryzae* reported by Agger and colleagues (4 μm; [41]), the initial mean spore projected area of 8.5 ± 0.1 μm^2 at inoculation corresponds to an equivalent spore diameter of 3.3 ± 0.4 μm. An increase in mean spore projected area of approximately 30% was observed from 0 to 6 h, corresponding to an increase in mean equivalent spore diameter of approximately 0.45 μm (and a linear swelling rate of 0.08 μm h^{-1}). Germ tube emergence from a large number of spores had occurred by 8 h, resulting in a circularity value of less than 0.8 and their consequent exclusion from the analysis. Removal of such large objects resulted in a decrease in the measured mean projected area at this time point. The circularity of the spores was found to remain relatively constant as projected area increased from 0 to

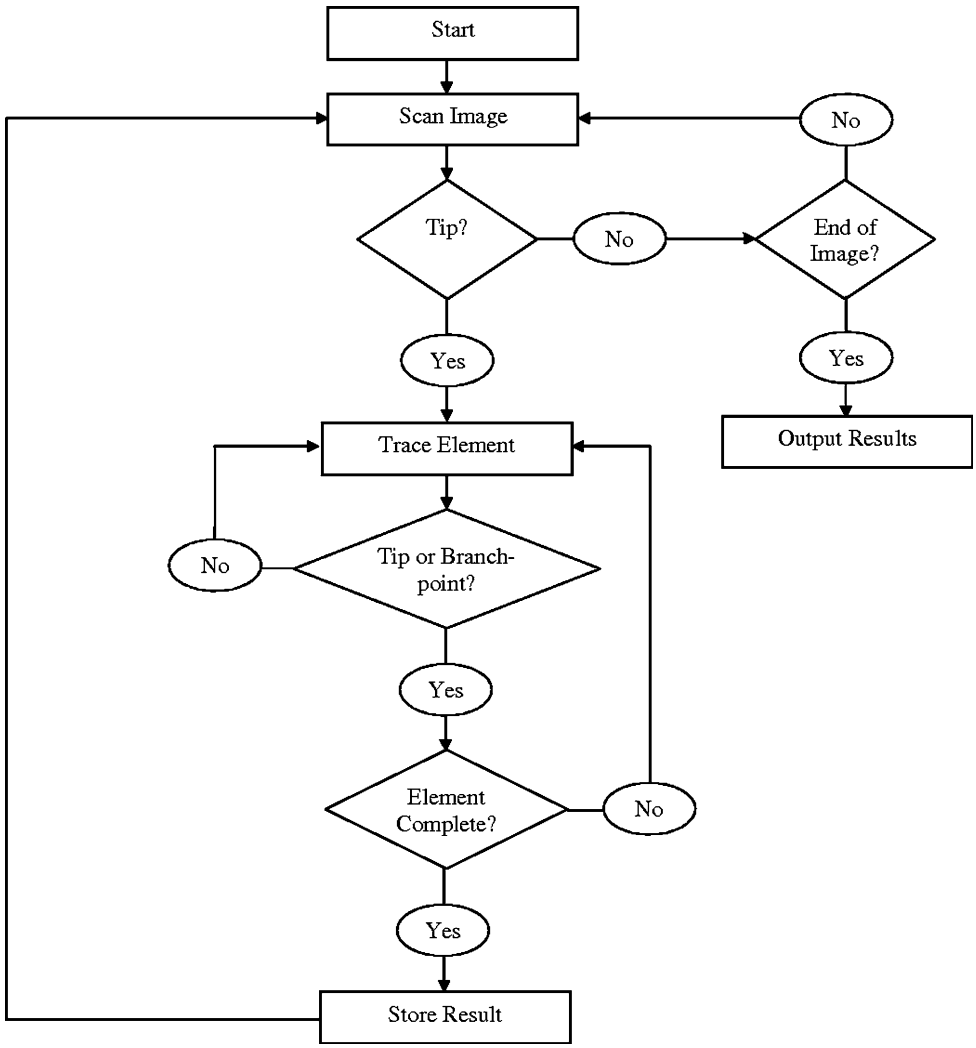

Fig. 4 Algorithm used for the analysis of skeletal hyphal elements

6 h, as previously reported for individual *A. oryzae* spores in submerged culture in a flow-through cell [33].

The mean projected area of spores may not give an accurate representation of the swelling process, as each sample was found to contain a wide range of spore sizes, particularly at later time points (Fig. 9). The projected area of most spores in the inoculum (0 h) was in the range 5–13 μm^2. Additionally, it was known from the routine preparation of spore stock suspensions that approximately 60% of spores were non-viable when thawed from frozen (as judged by a failure to germinate over 48 h during the total viable count procedure on malt agar, compared with an original total count performed using a Neubauer chamber). After incubation for 8 h, the projected area of such non-viable spores should not have increased, and it is reasonable to assume that most non-viable spores still occupied the size range of 5–13 μm^2. However, the possibility of viable spores exhibiting a small projected area in the same range, even after 8 h, cannot be eliminated, as it is apparent from the size distributions that swelling rates can vary to a large extent among different spores. Consequently, excluding non-viable spores from the analysis is difficult to achieve, because they cannot be distinguished on the basis of size alone. Specifying a minimum projected area threshold to exclude these non-viable spores would most likely exclude an unknown number of viable spores from the analysis. Such a wide variation in spore sizes and swelling rates has previously been reported in the study of *Penicillium chrysogenum* in submerged culture [42].

It was found that small variations in the value of $C_{s,min}$ did not have a significant impact on the measured average spore projected area or mean spore circularity (Fig. 10). In the analysis of samples taken at 6 h, a decrease of 0.05 in the value of $C_{s,min}$ resulted in an increase of approximately 0.75 μm^2 in the measured mean spore projected area (for $C_{s,min}$ greater than 0.7). This is a result of a greater number of clumped spores (relatively large artefacts) being included in the analysis as the circularity threshold is lowered. This variation may be reduced by placing an upper limit on the projected area of objects included in the analysis.

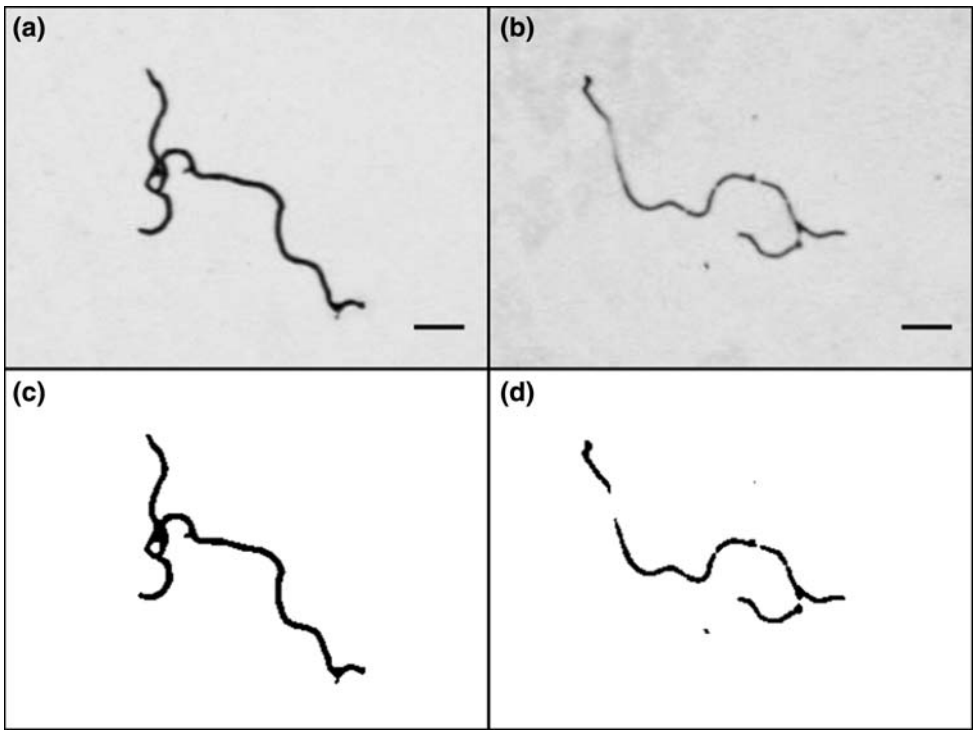

Fig. 5 Staining wet membranes resulted in non-uniform stain uptake. **a** Samples of *A. oryzae* on cellulose nitrate membranes were fixed and then dried at 65°C for 75 min prior to staining; **b** Samples were stained while wet immediately upon removal from agar surface. **c** Binary image resulting from grey-level thresholding of "**a**" (a single hyphal structure produced); **d** Binary image of "**b**" (six distinct structures are produced). *Bar* 30 μm

Table 1 Effect of drying time and temperature on spore morphology

Drying temperature (°C)	Drying time (h)	Mean projected area (μm^2)	Mean circularity	*n*
25	0	7.7 ± 0.3	0.895 ± 0.003	726
25[a]	24	8.2 ± 0.3	0.888 ± 0.003	2,915
25	72	7.1 ± 0.2	0.882 ± 0.003	768
65	1.25	8.4 ± 0.1	0.887 ± 0.002	2,505
105	0.17	8.4 ± 0.1	0.886 ± 0.002	2,315

Mean projected area and mean circularity of *A. oryzae* spores subjected to various drying treatments prior to staining. Errors represent 95% confidence intervals

[a] Average of two independent experiments

Reducing the value of $C_{s,min}$ also had the effect of reducing the mean spore circularity at each time-point, as objects of a lower circularity are included in the analysis. In the analysis of samples taken at 6 h, a decrease of 0.05 in the value of $C_{s,min}$ resulted in a decrease of approximately 0.02 in the measured mean spore circularity.

Kinetics of hyphal growth

The development of *A. oryzae* hyphal elements was characterised over a 10-h period from 14 to 24 h after inoculation, using both automatic and semi-automatic image analysis (Fig. 11). Similar results were obtained using either method to determine the mean values for total hyphal length, the number of tips, and the hyphal growth unit. Assuming hyphae to be cylinders of approximately constant radius (r) and density (ρ), then biomass (x) is directly proportional to the total hyphal length (l_h):

$$X = \pi r^2 \rho l_h$$

The specific growth rate (μ) can then be estimated according to:

$$\mu = 2.3(\log_{10} l_h - \log_{10} l_{h_0})/t$$

where l_h is the total hyphal length at time t and l_{h_0} is the total hyphal length at time $t = 0$. A value of approximately 0.27 h^{-1} was calculated for μ on the basis of data acquired using semi-automatic image analysis and 0.24 h^{-1} for the fully automatic method. Specific growth rates were calculated on the basis of total hyphal length in the study of *A. oryzae* in a flow-through cell [33], where the immersion of the fungus in a glucose-rich medium resulted in values of μ of up to 0.37 h^{-1}. The hyphal growth unit can be seen to be tending towards a constant value of approximately 72 ± 8 μm.

A large distribution in the size of individual hyphal elements was observed at each time-point, with the

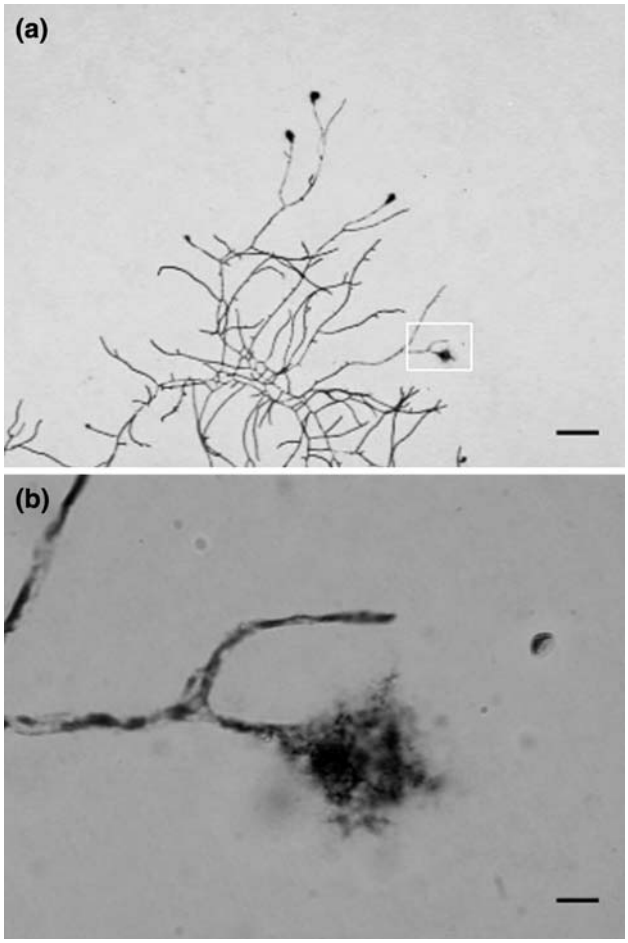

Fig. 6 Appearance of hyphal tips of *Aspergillus oryzae* when samples are dried without fixative prior to staining. **a** 100×; *bar* 100 μm. **b** 1000×; *bar* 10 μm

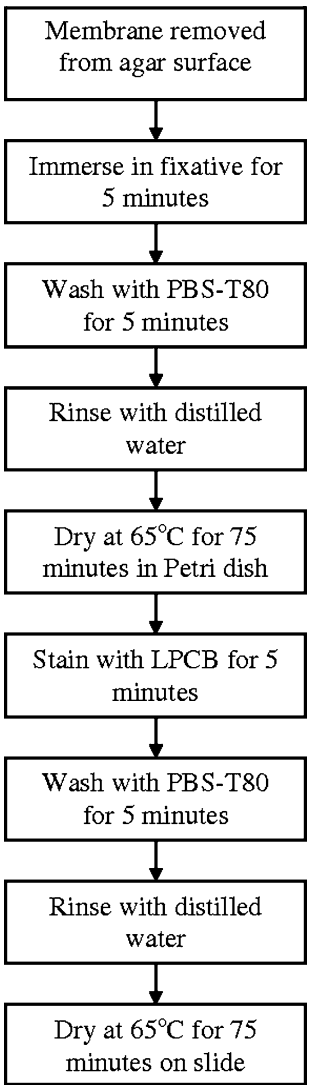

Fig. 7 Optimised procedure for processing of cultured cellulose nitrate membranes for image analysis

distribution being greatest in the later stages of the analysis (Fig. 12). This may be a result of variations in the specific growth rate of different hyphal elements within a given sample. Differences in spore swelling rate and germination time would also make a significant contribution to the observed variation in the sizes. Considering the increase in total hyphal length as an exponential function, a difference of as little as 10% in the specific growth rate of two hyphal elements would result in a significant variation in total hyphal length after 24 h of growth. Variations in the specific growth rate well in excess of this figure have been reported in an online study of *A. oryzae* in submerged culture [33].

The effect of varying $C_{h,max}$ by ± 0.10 was tested and was found to have little influence on the results (Fig. 13). Reducing the value of $C_{h,max}$ will have the effect of excluding a greater number of artefacts from the analysis. However, it will also result in the exclusion of small unbranched hyphae, which typically have a circularity of 0.3–0.4, depending on their size. By excluding these small hyphae from the analysis, the mean total hyphal length and the mean number of tips per hyphal element will be slightly over-estimated, particularly for earlier time-points.

The effect of varying $L_{b,min}$ by ±2 μm was also tested and was found to have little influence on the measured mean number of tips (Fig. 14) and virtually no influence on the mean total hyphal length (not shown). Increasing the value of $L_{b,min}$ will result in smaller branches being excluded from the analysis and an underestimation in the number of tips. A large increase in the value of $L_{b,min}$ would be necessary to cause a significant decrease in the mean total hyphal length. Removing branches of 2–4 μm in length is unlikely to have a significant effect on the final result when analysing structures with a total length that is hundreds, or even thousands, of microns in length.

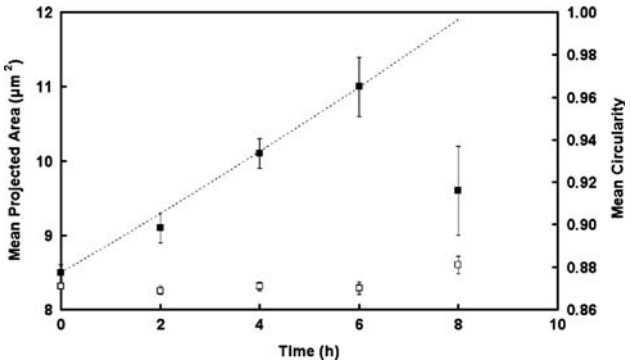

Fig. 8 Mean projected area (*filled squares*) and mean circularity (*empty squares*) of *A. oryzae* spores incubated on cellulose nitrate membranes on malt agar at 25°C. $A_{p,min} = 3\ \mu m^2$, $C_{s,min} = 0.8$. The increase in mean equivalent spore diameter was approximately linear at a rate of 0.08 μm h^{-1} (*dotted line*). An average of approximately 1,500 spores were analysed per time-point from 0 to 6 h and 350 at 8 h. *Error bars* represent 95% confidence intervals

Discussion

The routine translation of morphological data into actionable bioprocess strategies remains a priority target in industrial fungal fermentation. Computer-aided image analysis is an essential enabling tool in achieving this goal. Two complementary approaches may be discerned in the literature to reconcile the complexity of a typical vegetative mycelium with the practical limitations of imaging technology. The detailed analysis of a small number of individual hyphal elements in both submerged [33, 43] and solid-state culture systems [44, 45] has contributed much to our understanding of apical growth processes. An alternative approach, aimed at process optimization within bioreactor systems, has been to derive average data from large cell populations [42], with extension of the analysis to a consideration of both micromorphological and macromorphological forms [18].

In this study a new system has been presented for quantitative analysis of spore and hyphal morphology. The method obviates the need for purchase of relatively expensive commercial image-analysis software by adding utility on to the publicly available ImageJ platform, a system of proven usefulness in this field [46, 47]. Using *A. oryzae* as a model fungus, and building on earlier work demonstrating the utility of cellulose-based membranes for high-magnification, microscopic examination of fungi [39], new ImageJ plug-ins have been validated for study of early-stage development of the fungus. In presenting complex fungal conformations in an essentially two-dimensional format, membrane immobilization confines

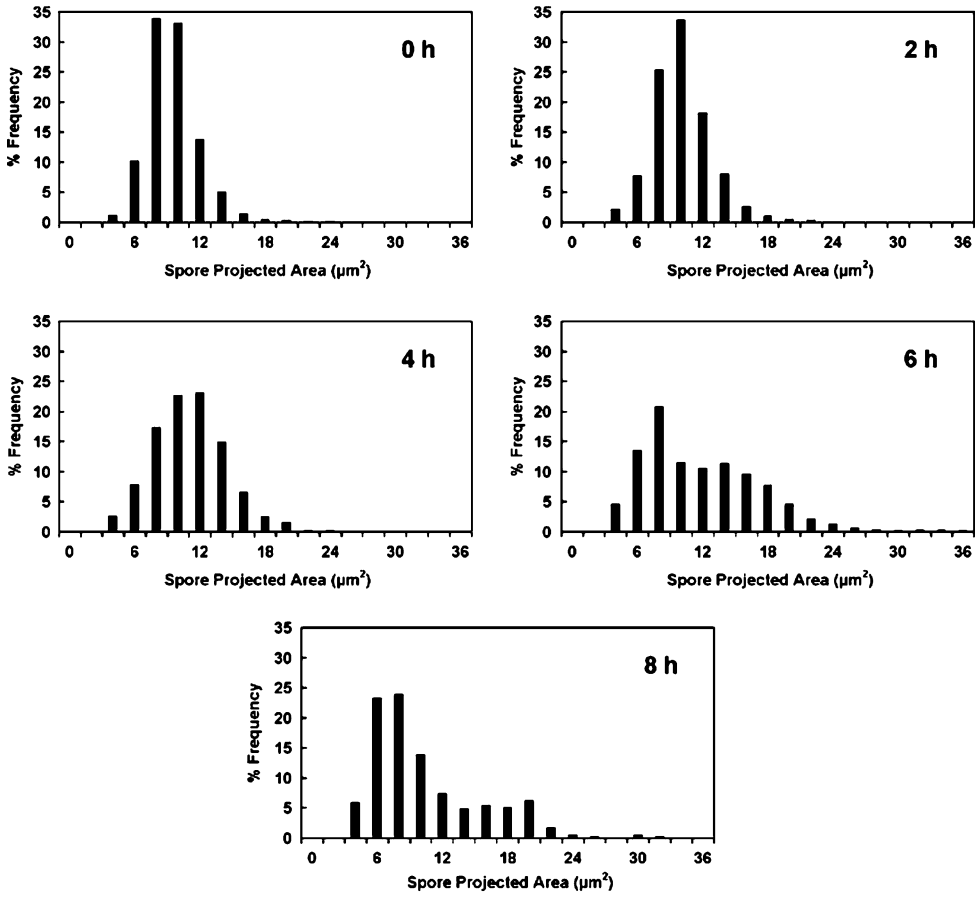

Fig. 9 Comparisons of size distributions of populations of *A. oryzae* spores. Spores were incubated on mixed cellulose ester membranes on malt agar at 25°C and analyzed at the time intervals shown. $A_{p,min} = 3\ \mu m^2$, $C_{s,min} = 0.8$

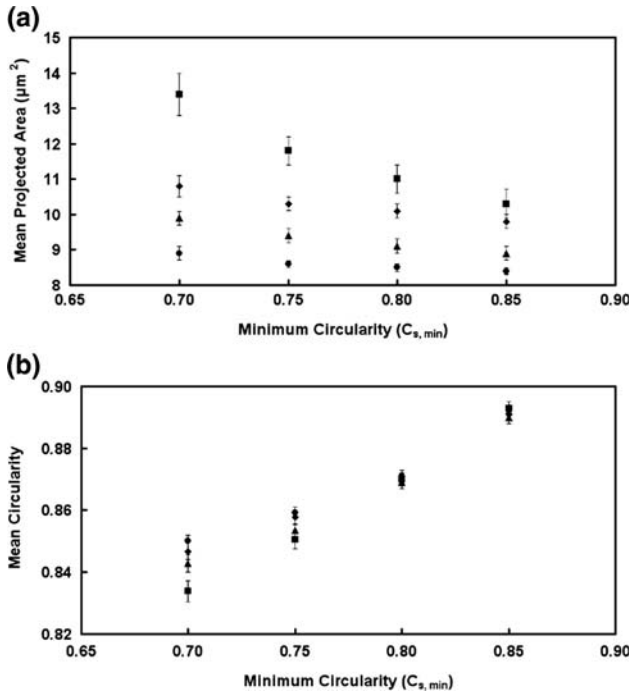

Fig. 10 Variations in mean spore projected area (**a**) and mean spore circularity (**b**) at different time intervals. Automatic image analysis was performed for different values of $C_{s,min}$. The times used were 0 (*circles*), 2 (*triangles*), 4 (*diamonds*) and 6 (*squares*) h. *Error bars* represent 95% confidence intervals

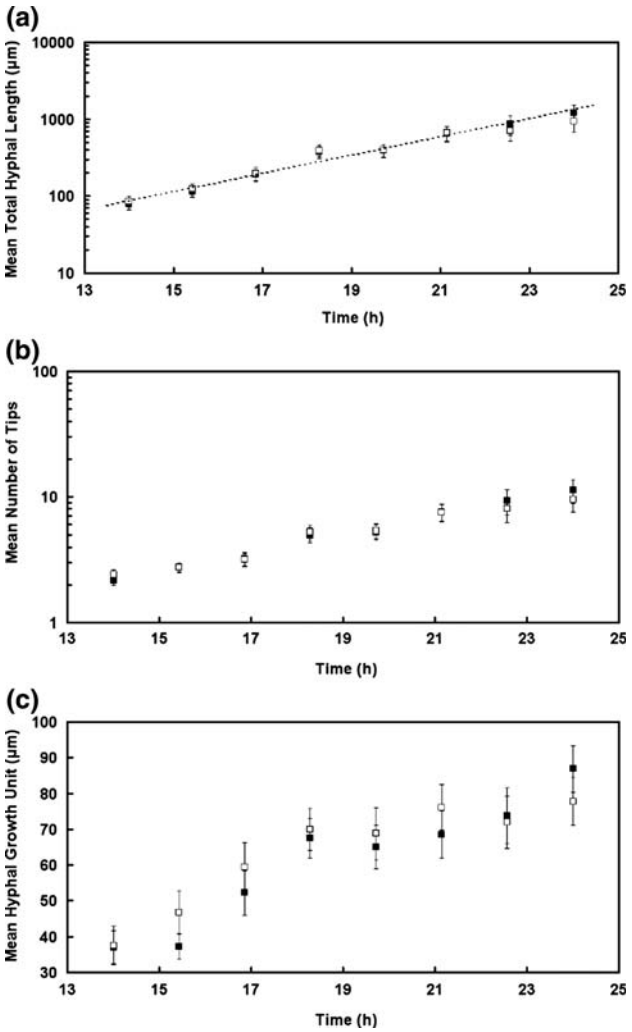

Fig. 11 Growth kinetics of *A. oryzae* on malt agar as determined by semi-automatic (*filled squares*) and automatic (*empty squares*) image analysis. $L_{b,min} = 2.5$ μm and $C_{h,max} = 0.35$. **a** Mean total hyphal length; the *dotted line* represents exponential growth with a specific growth rate of 0.27 h^{-1}. **b** Mean number of tips. **c** Mean hyphal growth unit. Approximately 100 elements were analysed for each time-point. *Error bars* represent 95% confidence intervals

cultures to a single focal plane, while being directly relevant to maintaining the natural spatial arrangement of vegetative mycelia encountered in solid state culture. Archiving of membrane-bound material is also possible, as the culture is fixed, stained, and killed during specimen preparation. It has been found that samples stored for up to two years after preparation are still suitable for imaging. Work is currently underway to extend the system to submerged culture systems by filtering liquid phase mycelial samples through cellulose nitrate filters for subsequent analysis.

In common with all image-analysis systems, the analysis routines described here depend on high-quality input images and are sensitive to elevated levels of artefact, which may result if large amounts of sediment are present in solutions used during filtration. The image-analysis system has some difficulty in distinguishing between "young" hyphae (recently germinated spores) and spore clusters, because of their morphological similarity in terms of projected area and circularity (in the approximate range 0.4–0.8). As such, these young hyphae and spore clusters are typically excluded from the analysis. In order to fully characterise this transition from spore to hypha, a means of distinguishing between these different objects is required. Boundary shape descriptors [48, 49] could be utilised in conjunction with the morphological thresholds used in the current study to this end. A means of breaking up clumps of spores in the inoculum, such as sonication, may also help to alleviate the problem.

Membranes have previously been used to analyse the growth of fungi on solid substrates and have been combined with image analysis and light microscopy, but generally with low magnification, low resolution capability. Cellulose acetate membranes have been used to study the growth of *Trichoderma virens* [50] in conjunction with a dissecting microscope. Image analysis has been used in the enumeration of the fractal dimension of *Pycnoporus cinnabarinus* [51] and *Trichoderma viride* [52] colonies immobilized on polycarbonate and cellophane membranes, respectively. The quantification of septation in *Streptomyces tendae* was

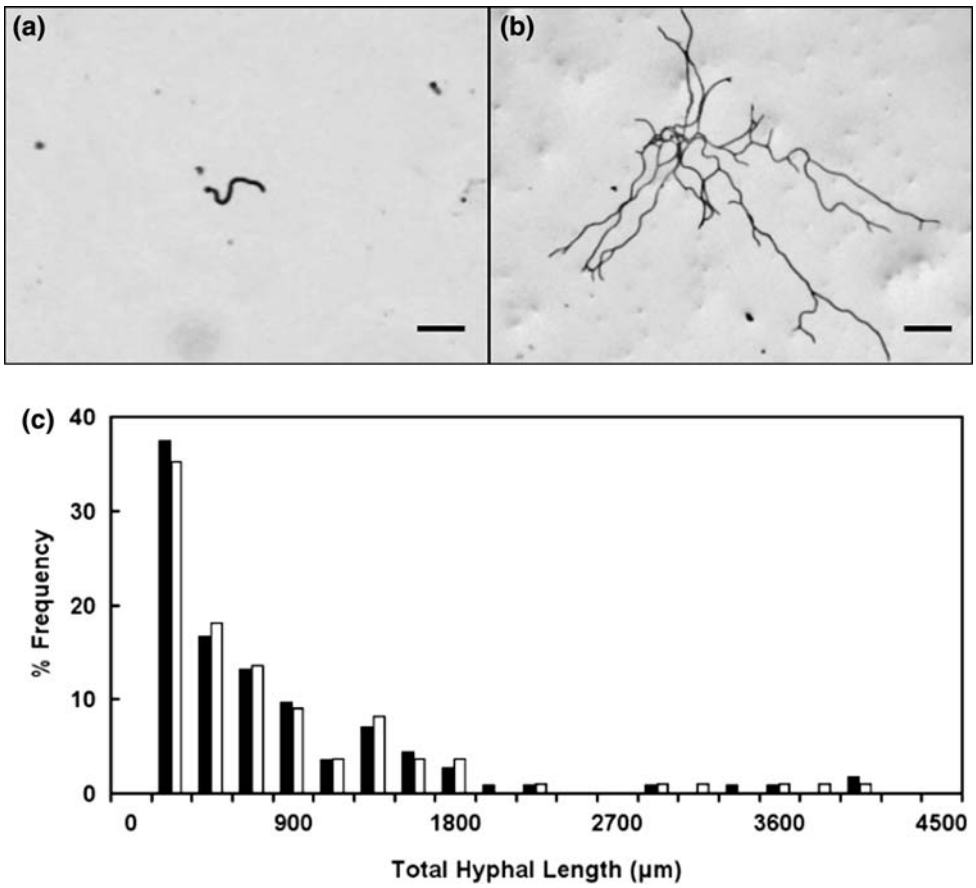

Fig. 12 Images taken from the same 21-hour old sample of *A. oryzae* cultivated on cellulose nitrate membranes on malt agar show a wide variation in total hyphal length. *Bar lengths*: **a** 40 µm, **b** 100 µm, **c** Distribution of total hyphal lengths in a sample of *A. oryzae* taken 21 h after inoculation on malt agar, as determined by semi-automatic image analysis (*filled columns*) and automatic image analysis with $L_{b,min} = 2.5$, $C_{h,max} = 0.35$ (*empty columns*)

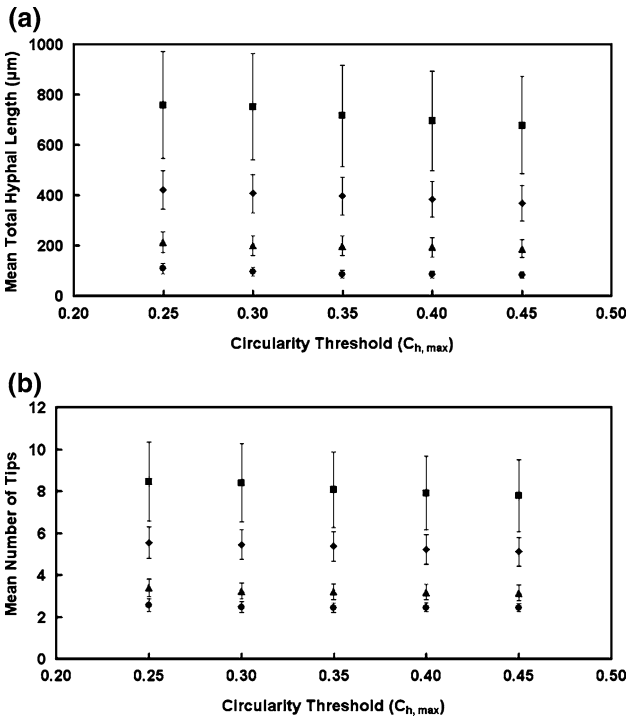

Fig. 13 Variations in mean total hyphal length **a** and mean number of tips **b** at different time intervals. Automatic image analysis was performed for different values of $C_{h,max}$. The times used were 14 (*circles*), 16.9 (*triangles*), 19.7 (*diamonds*), and 22.6 (*squares*) h. *Error bars* represent 95% confidence intervals

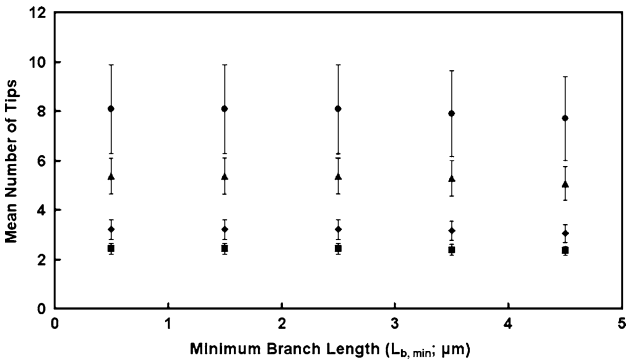

Fig. 14 Variations in mean number of tips as determined by automatic image analysis for different values of $L_{b,min}$. The times used were 14 (*circles*), 16.9 (*triangles*), 19.7 (*diamonds*) and 22.6 (*squares*) h. *Error bars* represent 95% confidence intervals

achieved using cellophane membranes in conjunction with image analysis [53], but this method involved the highly skilful transfer of mycelial matter from the membrane to a microscope slide for analysis.

The processing time of the image-analysis system of approximately 1 s per image (640 × 480 pixels) enables rapid quantification of fungal morphology. An analysis of a large bank of images and the subsequent calculation of properties such as spore swelling rate, hyphal growth rate,

and hyphal branching rate can be achieved in a matter of minutes, excluding the time necessary for image capture. In the analysis of each hyphal element, the coordinates of each tip and branch-point are recorded. This information could be used to geometrically map the foraging strategies of fungi on solid substrates, which has been previously studied using the calculation of the local fractal dimension within a colony [52]. Additionally, the recording of the length of each individual "segment" of the hyphal element enables compilation of size distributions of branches and inter-branch segments, enabling more accurate characterization of the branching strategy of the organism beyond the conventional hyphal growth unit.

Conclusion

Given the demonstrated relationship between morphology and productivity in industrial fungal fermentation processes, there is a need for development of automated image-analysis techniques for accurate and rapid quantification of this fundamental bioprocess characteristic. While tremendous progress has been made in this area in recent years, many of the reported techniques are specific to the submerged culture format. Those techniques that have been developed for the analysis of solid-state cultures have generally focussed on the macro-morphological form of fungal colonies, quantifying global properties such as fractal dimension and area coverage. The method presented here enables high-resolution characterization of early fungal development from the time of inoculation. It is hoped that the use of this technique will lead to a greater understanding of fungal growth kinetics and their relationship to macro-morphological forms and productivity in industrial fermentation processes.

Acknowledgements This work has been supported by a grant from the Technological Sector Research, Strand 1 Postgraduate R&D Skills Programme. We thank P. Taylor for her technical assistance in this study.

References

1. Rodriguez-Tudela JL, Aviles P (1991) Improved adhesive method for microscopic examination of fungi in culture. J Clin Microbiol 29:2604–2605
2. Harris JL (2000) Safe, low-distortion tape touch method for fungal slide mounts. J Clin Microbiol 38:4683–4684
3. Wang L, Ridgway D, Gu T, Moo-Young M (2005) Bioprocessing strategies to improve heterologous protein production in filamentous fungal fermentations. Biotechnol Adv 23:115–129. doi:10.1016/j.biotechadv.2004.11.001
4. Kim Y, Nandakumar MP, Marten MR (2007) Proteomics of filamentous fungi. Trends Biotechnol 25:395–400. doi:10.1016/j.tibtech.2007.07.008
5. Gerngross TU (2004) Advances in the production of human therapeutic proteins in yeasts and filamentous fungi. Nat Biotechnol 22:1409–1414. doi:10.1038/nbt1028
6. Mitchell DA (1992) Growth patterns, growth kinetics and the modelling of growth in solid-state cultivation. In: Doelle HW, Mitchell DA, Rolz C (eds) Solid substrate cultivation. Elsevier Applied Science, New York, pp 87–114
7. Ishida H, Hata Y, Kawato A, Abe Y, Suginami K, Imayasu S (2000) Identification of functional elements that regulate the glucoamylase-encoding gene (glaB) expressed in solid-state culture of *Aspergillus oryzae*. Curr Genet 37:373–379. doi:10.1007/s002940000118
8. Iwashita K (2002) Recent studies of protein secretion by filamentous fungi. J Biosci Bioeng 94:530–535
9. te Biesebeke R, Ruijter G, Rahardjo YSP, Hoogschagen MJ, Heerikhuisen M, Levin A, van Driel KGA, Schutyser MAI, Dijksterhuis J, Zhu Y, Weber FJ, de Vos WM, van den Hondel KAMJJ, Rinzema A, Punt PJ (2002) *Aspergillus oryzae* in solid-state and submerged fermentations. FEM Yeast Res 2:245–248
10. Bigelis R, He H, Yang HY, Chang LP, Greenstein M (2006) Production of fungal antibiotics using polymeric solid supports in solid-state and liquid fermentation. J Ind Microbiol Biotechnol 33:815–826. doi:10.1007/s10295-006-0126-z
11. Oda K, Kakizono D, Yamada O, Iefuji H, Akita O, Iwashita K (2006) Proteomic analysis of extracellular proteins from *Aspergillus oryzae* grown under submerged and solid-state culture conditions. Appl Environ Microbiol 72:3448–3457. doi:10.1128/AEM.72.5.3448-3457.2006
12. Papagianni M (2004) Fungal morphology and metabolite production in submerged mycelial processes. Biotechnol Adv 22:189–259. doi:10.1016/j.biotechadv.2003.09.005
13. Wessels JGH (1993) Tansley Review No. 45. Wall growth, protein excretion and morphogenesis in fungi. New Phytol 123:397–413. doi:10.1111/j.1469-8137.1993.tb03751.x
14. Gordon CL, Archer DB, Jeenes DJ, Doonan JH, Wells B, Trinci AP, Robson GD (2000) A glucoamylase:GFP gene fusion to study protein secretion by individual hyphae of *Aspergillus niger*. J Microbiol Methods 42:39–48. doi:10.1016/S0167-7012(00)00170-6
15. Muller C, McIntyre M, Hansen K, Nielsen J (2002) Metabolic engineering of the morphology of *Aspergillus oryzae* by altering chitin synthesis. Appl Environ Microbiol 68:1827–1836. doi:10.1128/AEM.68.4.1827-1836.2002
16. Papagianni M, Mattey M, Kristiansen B (1999) Hyphal vacuolation and fragmentation in batch and fed-batch culture of *Aspergillus niger* and its relation to citric acid production. Process Biochem 35:359–366. doi:10.1016/S0032-9592(99)00079-5
17. Muller C, Spohr AB, Nielsen J (2000) Role of substrate concentration in mitosis and hyphal extension of *Aspergillus*. Biotechnol Bioeng 67:390–397. doi:10.1002/(SICI)1097-0290(20000220)67:4<390::AID-BIT2>3.0.CO;2-O
18. Cox PW, Paul GC, Thomas CR (1998) Image analysis of the morphology of filamentous micro-organisms. Microbiology 144(Pt 4):817–827
19. Amanullah A, Blair R, Nienow AW, Thomas CR (1999) Effects of agitation intensity on mycelial morphology and protein production in chemostat cultures of recombinant *Aspergillus oryzae*. Biotechnol Bioeng 62:434–446. doi:10.1002/(SICI)1097-0290(19990220)62:4<;434::AID-BIT6>;3.0.CO;2-D
20. Metz B, Kossen NWF (1977) The growth of molds in the form of pellets—a literature review. Biotechnol Bioeng 19:781–799. doi:10.1002/bit.260190602
21. Zetelaki K, Vas K (1968) The role of aeration and agitation in the production of glucose oxidase in submerged culture. Biotechnol Bioeng 10:45–59. doi:10.1002/bit.260100104

22. Hermersdörfer H, Leuchtenberger A, Wardsack C, Ruttloff H (1987) Influence of culture conditions on mycelial structure and polygalacturonase synthesis of *Aspergillus niger*. J Basic Microbiol 27:309–315. doi:10.1002/jobm.3620270604
23. Papagianni M, Moo-Young M (2002) Protease secretion in glucoamylase producer *Aspergillus niger* cultures: fungal morphology and inoculum effects. Process Biochem 37:1271–1278. doi:10.1016/S0032-9592(02)00002-X
24. Kisser M, Kubicek CP, Röhr M (1980) Influence of manganese on morphology and cell wall composition of *Aspergillus niger* during citric acid fermentation. Arch Microbiol 128:26–33. doi:10.1007/BF00422301
25. Paul GC, Priede MA, Thomas CR (1999) Relationship between morphology and citric acid production in submerged *Aspergillus niger* fermentations. Biochem Eng J 3:121–129. doi:10.1016/S1369-703X(99)00012-1
26. Žnidaršič P, Pavko A (2001) The morphology of filamentous fungi in submerged cultivations as a bioprocess parameter. Food Technol Biotechnol 39:237–252
27. Elmayergi H, Scharer JM, Moo-Young M (1973) Effects of polymer additives on fermentation parameters in a culture of *A. niger*. Biotechnol Bioeng 15:845–859. doi:10.1002/bit.260150503
28. Thibault J, Pouliot K, Agosin E, Pérez-Correa R (2000) Reassessment of the estimation of dissolved oxygen concentration profile and KLa in solid-state fermentation. Process Biochem 36:9–18. doi:10.1016/S0032-9592(00)00156-4
29. Couri S, Merces EP, Neves BC, Senna LF (2006) Digital image processing as a tool to monitor biomass growth in *Aspergillus niger* 3T5B8 solid-state fermentation: preliminary results. J Microsc 224:290–297. doi:10.1111/j.1365-2818.2006.01699.x
30. Caldwell IY, Trinci APJ (1973) The growth unit of the mould *Geotrichum candidum*. Arch Microbiol 88:1–10. doi:10.1007/BF00408836
31. Metz B, de Bruijn EW, van Suijdam JC (1981) Methods for quantitative representation of the morphology of molds. Biotechnol Bioeng 23:149–162. doi:10.1002/bit.260230110
32. Tucker KG, Kelly T, Delgrazia P, Thomas CR (1992) Fully-automatic measurement of mycelial morphology by image analysis. Biotechnol Prog 8:353–359. doi:10.1021/bp00016a013
33. Spohr A, Dam-Mikkelsen C, Carlsen M, Nielsen J, Villadsen J (1998) On-line study of fungal morphology during submerged growth in a small flow-through cell. Biotechnol Bioeng 58:541–553. doi:10.1002/(SICI)1097-0290(19980605)58:5<;541::AID-BIT11>;3.0.CO;2-E
34. El-Sabbagh N, McNeil B, Harvey LM (2006) Dissolved carbon dioxide effects on growth, nutrient consumption, penicillin synthesis and morphology in batch cultures of *Penicillium chrysogenum*. Enzyme Microb Technol 39:185–190. doi:10.1016/j.enzmictec.2005.10.020
35. Packer HL, Thomas CR (1990) Morphological measurements on filamentous microorganisms by fully automatic image analysis. Biotechnol Bioeng 35:870–881. doi:10.1002/bit.260350904
36. Obert M, Pfeifer P, Sernetz M (1990) Microbial growth patterns described by fractal geometry. J Bacteriol 172:1180–1185
37. Li ZJ, Shukla V, Wenger KS, Fordyce AP, Pedersen AG, Marten MR (2002) Effects of increased impeller power in a production-scale *Aspergillus oryzae* fermentation. Biotechnol Prog 18:437–444. doi:10.1021/bp020023c
38. Papagianni M, Mattey M (2006) Morphological development of *Aspergillus niger* in submerged citric acid fermentation as a function of the spore inoculum level. Application of neural network and cluster analysis for characterization of mycelial morphology. Microb Cell Fact 5:3. doi:10.1186/1475-2859-5-3
39. Barry DJ, Chan C, Williams GA (2007) Nitrocellulose as a general tool for fungal slide mounts. J Clin Microbiol 45:1074–1075. doi:10.1128/JCM.01609-06
40. Drouin JF, Louvel L, Vanhoutte B, Vivier H, Pons MN, Germain P (1997) Quantitative characterization of cellular differentiation of *Streptomyces ambofaciens* in submerged culture by image analysis. Biotechnol Tech V11:819–824. doi:10.1023/A:1018429425800
41. Agger T, Spohr AB, Carlsen M, Nielsen J (1998) Growth and product formation of *Aspergillus oryzae* during submerged cultivations: verification of a morphologically structured model using fluorescent probes. Biotechnol Bioeng 57:321–329. doi:10.1002/(SICI)1097-0290(19980205)57:3<;321::AID-BIT9>;3.0.CO;2-J
42. Paul GC, Kent CA, Thomas CR (1993) Viability testing and characterization of germination of fungal spores by automatic image analysis. Biotechnol Bioeng 42:11–23. doi:10.1002/bit.260420103
43. Christiansen T, Spohr AB, Nielsen J (1999) On-line study of growth kinetics of single hyphae of *Aspergillus oryzae* in a flow-through cell. Biotechnol Bioeng 63:147–153. doi:10.1002/(SICI)1097-0290(19990420)63:2<;147::AID-BIT3>;3.0.CO;2-M
44. Bartnicki-Garcia S, Bracker CE, Gierz G, Lopez-Franco R, Lu H (2000) Mapping the growth of fungal hyphae: orthogonal cell wall expansion during tip growth and the role of turgor. Biophys J 79:2382–2390
45. Dieguez-Uribeondo J, Gierz G, Bartnicki-Garcia S (2004) Image analysis of hyphal morphogenesis in *Saprolegniaceae* (Oomycetes). Fungal Genet Biol 41:293–307. doi:10.1016/j.fgb.2003.10.012
46. Rahardjo YS, Sie S, Weber FJ, Tramper J, Rinzema A (2005) Effect of low oxygen concentrations on growth and alpha-amylase production of *Aspergillus oryzae* in model solid-state fermentation systems. Biomol Eng 21:163–172
47. Papagianni M (2006) Quantification of the fractal nature of mycelial aggregation in *Aspergillus niger* submerged cultures. Microb Cell Fact 5:5. doi:10.1186/1475-2859-5-5
48. Wilson J (2002) Towards the automated evaluation of crystallization trials. Acta Crystallogr D Biol Crystallogr 58:1907–1914. doi:10.1107/S0907444902016633
49. Pazoti MA, Garcia RE, Pessoa JDC, Bruno OM (2005) Comparison of shape analysis methods for *Guinardia citricarpa* ascospore characterization. Electron J Biotechnol 8:3
50. Cross D, Kenerley CM (2004) Modelling the growth of *Trichoderma virens* with limited sampling of digital images. J Appl Microbiol 97:486–494. doi:10.1111/j.1365-2672.2004.02310.x
51. Jones CL (1996) 2-D wavelet packet analysis of structural self-organisation and morphogenic regulation in filamentous fungal colonies. Complex Int 3:1
52. Hitchcock D, Glasbey CA, Ritz K (1996) Image analysis of space-filling by networks: application to a fungal mycelium. Biotechnol Tech 10:205–210. doi:10.1007/BF00158947
53. Reichl U, Yang H, Gilles ED, Wolf H (1990) An improved method for measuring the interseptal spacing in hyphae of *Streptomyces tendae* by fluorescence microscopy coupled with image processing. FEMS Microbiol Lett 67:207–210. doi:10.1111/j.1574-6968.1990.tb13864.x